ADVANCED FUNCTIONAL MATERIALS
www.afm-journal.de

Wrapping up Metal–Organic Framework Crystals with Carbon Nanotubes

*Belén Lerma-Berlanga, Natalia M. Padial, Marta Galbiati, Isaac Brotons-Alcázar, Josep Albero, Hermenegildo García, Alicia Forment-Aliaga, Carolina R. Ganivet, and Carlos Martí-Gastaldo**

The presence of tetrazine units in the organic nodes of UiO-68-TZCD controls the formation of ultrathin coatings of single-wall nanotubes that decorate the surface of the crystal. These crystal hybrids can be prepared straightforwardly in one step and are extraordinarily respectful with the properties of the framework for combination of mesoporosity and surface areas ≈4.000 $m^2 g^{-1}$, with excellent stability in water, and conductivities at room temperature of 4×10^{-2} S cm^{-1} even at very low carbon weight contents (2.3 wt.%).

1. Introduction

Metal–Organic Frameworks (MOFs) have gained increasing attention in fields like chemistry, biology, and materials science due to their unparalleled adaptability to different goals thanks to their modular nature.[1] These hybrid reticular solids, built from the interlinking of inorganic and organic nodes, offer periodic structures for tailorable porosity, pore chemistry, and structural diversity.[2] However, MOFs can also suffer from weak chemical (hydrolytic), thermal and mechanical stabilities,[3] complicated processability,[4] and poor electrical conductivity,[5,6] which limit their potential in fields as energy storage and conversion. In this regard, the preparation of composites by integration with other functional materials as polymers, metal nanoparticles, oxides, biomolecules, graphene, or carbon nanotubes (CNTs) is a powerful route to overcome some of these limitations. The combination, or even synergistic interaction of these components with the intrinsic properties of the MOF, can enable advanced performance of the resulting composites in proton transport,[7] H_2 photogeneration[8] or catalysis.[9] The intrinsic hydrophobicity and extraordinary mechanical and electrical properties of CNTs make them particularly appealing in this context.[10] CNT@MOF composites are often prepared by the addition of pre-formed MOF particles to bundles of nanotubes (ex situ) or directly synthesized in their presence (in situ). This results in the formation of necklace-like hybrids for an irregular distribution of MOF particles that are deposited/grown on top of the carbon matrix (**Figure 1**a). Oxidized CNTs incorporating superficial -OH and -CO_2H groups that act as nucleation sites are used to favor the growth of MOF nuclei. However, this often leads to unsought changes in the intrinsic properties of pristine nanotubes and is not sufficient to prevent the aggregation of MOF particles, control their distribution, or enable effective pathways for electronic hybridization. As beautifully illustrated for the case of MOF-polymer hybrids,[11] a better integration mediated by strong covalent linkages that were respectful with the intrinsic properties of both components would be arguably ideal to gain control over interfacial compatibility.

We recently described the use of tetrazine linkers as plug-and-play tags to enable metal-free click conjugation of several dienes, including fullerene, to porous frameworks by the inverse Electron-Demand Diels-Alder (iEDDA) reaction.[12] Here we demonstrate how this reactivity can be also used to achieve unprecedented control in the formation of very thin CNTs coatings decorating the surface of MOF crystals (Figure 1b).

B. Lerma-Berlanga, N. M. Padial, M. Galbiati, I. Brotons-Alcázar, C. R. Ganivet, C. Martí-Gastaldo
Instituto de Ciencia Molecular (ICMol)
Universitat de València
Paterna 46980, Spain
E-mail: carlos.marti@uv.es
J. Albero, H. García
Instituto Universitario de Tecnología Química CSIC-UPV
Universitat Politècnica de València
València 46022, Spain

The ORCID identification number(s) for the author(s) of this article can be found under https://doi.org/10.1002/adfm.202302246

DOI: 10.1002/adfm.202302246

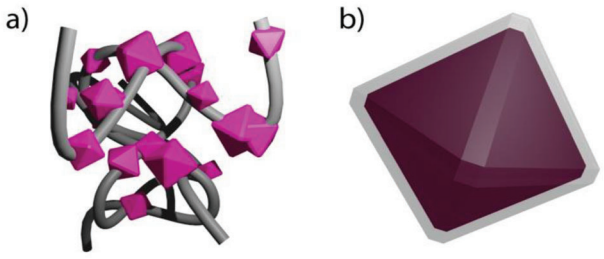

Figure 1. a) Hierarchical organization of CNT (grey) and MOF crystals (pink octahedra) in the composites obtained by conventional methodologies and b) MOF crystal hybrid prepared by conjugation of nanotubes to the crystal surface to form a permeable coating.

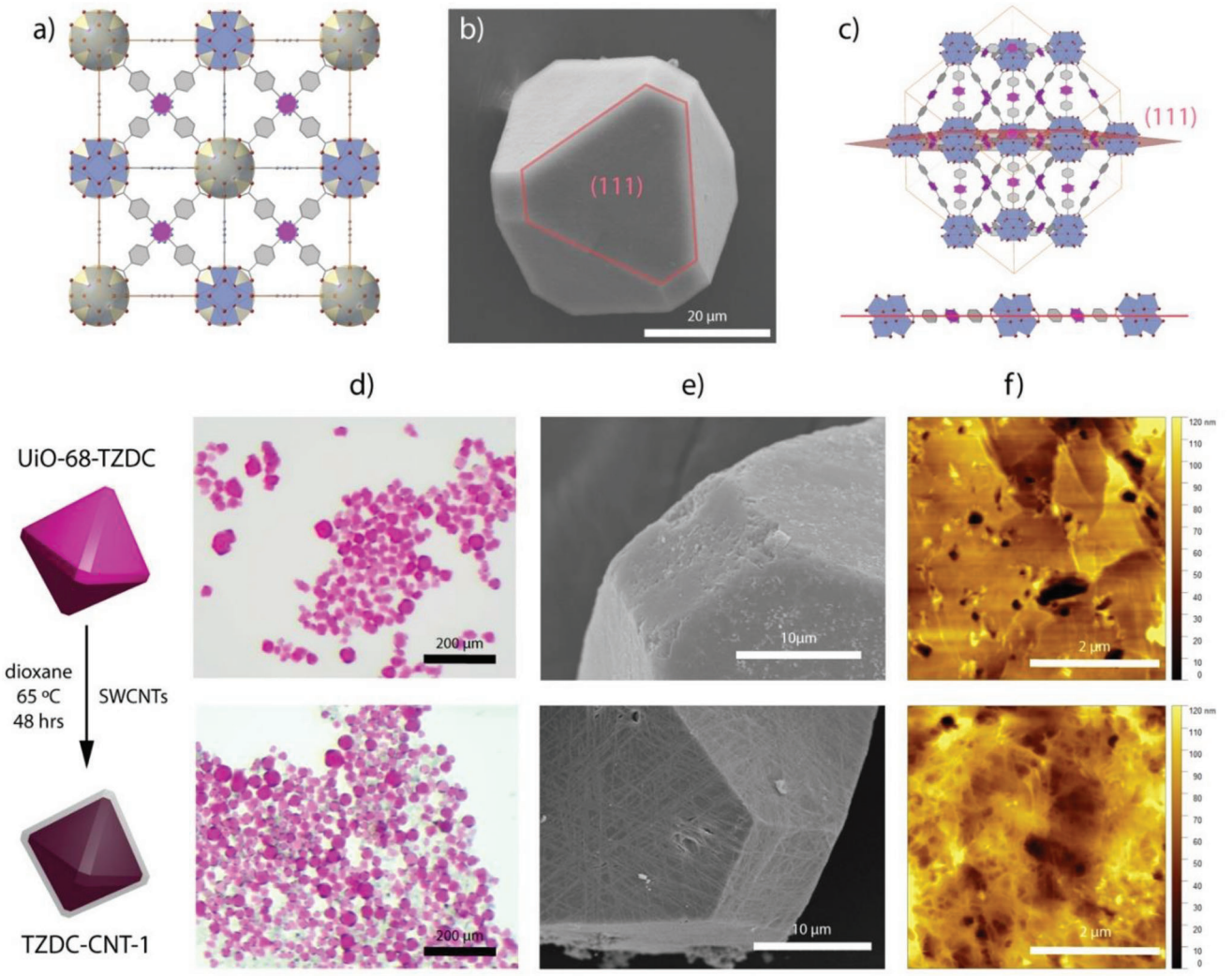

Figure 2. a) Structure of UiO-68-TZDC. Tetrazine units in the organic connectors are represented in pink. Pale yellow spheres represent mesoporous cavities. b) SEM picture showing the octahedral morphology of the crystal and the corresponding (111) crystallographic facets. c) Perspective of the unit cell shoving the cleavage plane (111) and the corresponding surface termination. Images of the crystals before (top) and after (bottom) reaction with SWCNTs by d) optical microscopy, e) SEM, and f) PeakForce Tapping Mode AFM.

Post-synthetic nanotube linkage proceeds at mild conditions, in one step, and is extraordinarily respectful with the properties of both components to enable the synthesis of mesoporous, electrically conductive CNT@MOF crystal hybrids.

2. Results and Discussion

UiO-68-TZDC is built from the assembly of 4,4'-(1,2,4,5-tetrazine-3,6-diyl)dibenzoic acid (H_2tzdc) linkers and 12-connected Zr_6 metal-oxo clusters (**Figure 2**a).[13] This open framework combines intrinsic mesoporosity with the availability of reactive tetrazine tags, ideal for bulk post-synthetic modification by reaction with dienophiles.[12] Also, the surface reactivity of these crystals will be dominated by the (111) facets of their truncated octahedral morphologies (Figure 2b). According to the cleavage of the crystal structure along this direction, this would correspond to tetrazine terminations ideally suited to surface functionalization (Figure 2c). These features make UiO-68-TZDC an ideal candidate to approach the grafting of CNTs. Compared to our previous work with small molecule dienophiles,[12] the low solubility and dispersibility in common organic solvents of the single-wall carbon nanotubes (SWCNTs) used in this case imposed specific changes to the experimental procedure. As a general procedure, a dispersion of SWCNTs in organic solvent was treated with ultrasounds followed by the addition of freshly made crystals of UiO-68-TZDC prepared according to our reported method.[13] The mixture was then incubated in an orbital shaker. The resulting slurry was separated from the organic solvent and redispersed in a 1:1 mixture of DMF:hexane with ultrasounds.

This facilitated isolating CNT@MOF crystals from the unreacted bundle of nanotubes. Experimental conditions were optimized by systematic screening of different solvents, CNT concentration, incubation temperature and time, and different reaction

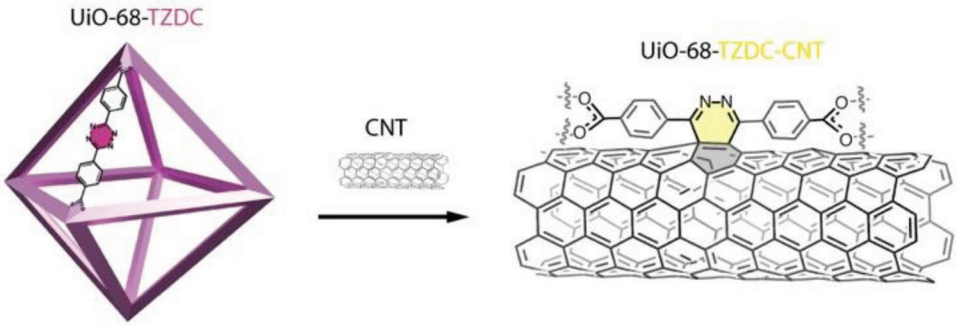

Scheme 1. Proposed linkage of CNT sidewall to the surface of tetrazine rings (pink) acting as electron-poor dienes in UiO-68-TZDC crystals by an inverse demand [4+2] Diels Alder reaction with the nanotube sidewall acting as electron-rich dienophiles (grey) for the formation of pyridazine rings (yellow) in the binding sites.

vessels (Sections S2.1 and S.2.2, Supporting Information). The impact of the conditions on the morphology of the crystal and the ease of purification due to variable dispersibility of the nanotubes in the solvents tested were considered as determining factors. Compared to toluene, *N,N*-dimethylformamide (DMF), or acetone, dioxane was the best choice for reaching a good compromise between CNT conjugation, minimum damage to the crystal, and facile purification. TZDC-CNT-1 was prepared by dispersing 80 mg of UiO-68-TZDC crystals in a suspension of 0.021 mg mL^{-1} of SWCNT in dioxane followed by incubation in a Schott glass bottle at 65 °C for 48 h (Section S2.3 , Supporting Information). Higher nanotube concentrations (0.062 mg mL^{-1}) led to visible aggregates on the surface of the crystals which difficulted separation and purification. In turn, the reaction time and temperature had a negligible effect on the final product. CNT conjugation was first analyzed by optical microscopy. Figure 2d shows how the pink octahedra characteristic of UiO-68-TZDC does not change significantly in color after the reaction, suggesting the formation of a very thin coating not visible at a single crystal level. Scanning Electron Microscopy (SEM) analysis of the surface of the crystals reveals clear differences. Compared to the pristine material that shows a bare surface, TZDC-CNT-1 confirms the formation of a clean coating layer with an internal structure reminiscent of a chainmail fabric (Figure 2e). The topography of the crystal surface was also analyzed with Atomic Force Microscopy (AFM). Single crystal images were captured in PeakForce Tapping Mode, placing the probe on top of the crystals and applying low force to ensure minimal effect over their surface (Figure 2f). Compared to the bare crystals, which present a rough surface with no observable terrace features indicative of a high supersaturation level during crystal growth,[14] TZDC-CNT-1 displays a dense array of intertwined nanotubes all over the surface which agrees well with the formation of a dense shell covering the crystal surface. We argue CNT conjugation in our case is facilitated by an inverse demand [4+2] DA reaction between the nanotube sidewall and the tetrazine rings in the surface of the crystal as summarized in **Scheme 1**. Similar sidewall functionalization of SWCNTs has been reported in solution,[15] and compatibility with mild conditions is enabled by the low thermodynamic stability of the resulting adducts facilitating spontaneous rearomatization.

The crucial role of tetrazine units in controlling nanotube conjugation was confirmed by testing the same reaction with UiO-68 crystals based on polyaromatic [1,1′:4′,1′′-terphenyl]-4,4′′-dicarboxylic acid (TPDC) linkers.[13] As expected, the absence of electron-poor tetrazine dienes in the TPDC linker resulted in a completely different behavior for unsuccessful grafting in all cases tested (Section S2.3, Supporting Information). We also explored the effect of more reactive dienophiles in inhibiting nanotube linkage by reacting CNTs and UiO-68-TZDC crystals in the same conditions after addition of an excess of 2,5-norbornadiene (NBD). SEM microscopy was used to discard the formation of a nanotube coating, suggesting that NBD inhibits the linkage of the less reactive dienophile in these conditions. This was further confirmed by ^{1}H-NMR analysis of the crystals after digestion in acid conditions, which confirms how the presence of NBD induces complete transformation of the tetrazine rings into pyridazine units,[12] thus preventing nanotube linkage (Section S2.3.3, Supporting Information).

Surface functionalization was next analyzed by Raman spectroscopy (**Figure 3**a). Compared to UiO-68-TZDC, only the spectrum of TZDC-CNT-1 displays vibrations at 234, 270, 1586, and 2576 cm^{-1} that can be associated respectively to the radial breathing modes (RMB), *G* and *G'* bands also present in pristine SWCNTs. The upward shift of ≈6 cm^{-1} in the breathing modes might be indicative of either covalent functionalization or the debundling of the nanotubes.[16] However, the detailed analysis of *D* band required to confirm covalent grafting was not possible due to the overlap of the Raman signal of the MOF in the corresponding frequency ranges. The formation of a surface coating was also confirmed by additional Raman spectra acquired from several crystal sections at variable penetration depth (Section S2.4.1, Supporting Information). X-ray photoelectron spectroscopy (XPS) was also used to analyze chemical changes in the surface of the crystal (Figure 3b). C/N ratios were calculated from the integrated areas of the C_{1s} and N_{1s} survey spectra peaks for each sample (Section S2.4.2, Supporting Information). Our data reveal an increase in the relative percentage of superficial carbon after the reaction consistent with the incorporation of CNTs to the surface of the crystal. The changes in carbon content are mainly concentrated in the surface of the crystal and can be clearly identified with a surface-sensitive technique as XPS. The use of bulk techniques as elemental CHN and thermogravimetric analysis (TGA) reveal small deviations compared to the pristine MOF, that account for a 0.6 wt.% content in nanotubes after the functionalization. This agrees well with the formation of a very thin coating. The structural integrity of the framework after reaction was con-

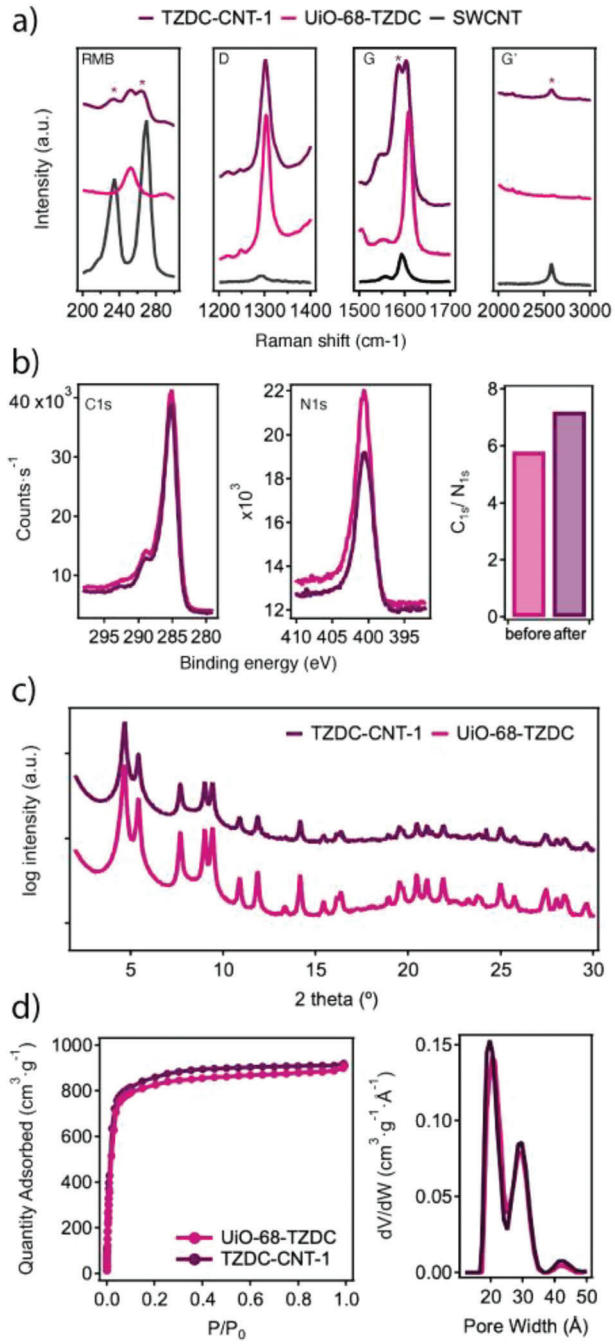

Figure 3. a) Raman spectra of UiO-68-TZDC and TZDC-CNT-1. RMB, *D*, *G*, and *G'* regions have been separated for clarity. b) XPS spectra of the crystals before and after CNT conjugation and corresponding increase in relative C%. c) PXRD in logarithmic scale of intensity. d) N_2 isotherms at 77 K and corresponding PSD plots analyzed with NLDFT kernel.

firmed with X-ray powder diffraction (PXRD, Figure 3c), for negligible changes to the unit cell parameters calculated by Le Bail refinement (Section S3.1, Supporting Information). Concerning the nanotubes, the absence of the characteristic broad diffraction at 25° is likely associated with the formation of a thin shell rather than aggregated bundles. Both materials were solvent-exchanged in hexane and evacuated at 10^{-6} torr overnight. They display almost identical non-hysteretic N_2 isotherms for BET surface areas (SA) ≈4150 $m^2\ g^{-1}$, and experimental pore size distributions (PSD) characteristic of UiO-68 type frameworks, revealing minimum impact to the crystal porosity (Figure 3d).

Our results confirm the formation of a thin and permeable CNT coating layer, that is exquisitely respectful with the intrinsic properties of the framework in terms of the structure, thermal stability, and accessible surface area of the resulting crystal composite. During the optimization of the synthesis of this hybrid, we noticed that the geometry of the reactor had an important effect on the aggregation of MOF crystals and nanotubes. We hypothesized this might induce variations in the local concentration for changes in the extent of functionalization. To test this possibility, we replaced Schott glass bottles with Wheaton culture tubes, featuring a curved base with a smaller area while keeping the same concentrations of nanotubes (0.019 mg mL^{-1}), and equivalent reaction conditions. Compared to TZDC-CNT-1, the color of these TZDC-CNT-2 crystals were slightly darker (**Figure 4**a). As summarized in Section S4 (Supporting Information), this hybrid was next analyzed with the same techniques described above to confirm the formation of equivalent but thicker coatings, for a higher net carbon content (2.3 wt.%) and a negligible impact on the porosity of the UiO-68-TZDC framework.

Contact angle measurements were used to test the hydrophobicity of the CNT@MOF hybrids (Figure 4b). Compared to the hydrophilicity of UiO-68-TZDC, TZDC-CNT-1 and 2 show exterior surface hydrophobicity for similar contact angles of 120 and 125 °. This surface wettability is comparable to that attained by using fluorinated linkers or post-synthetic coating with hydrophobic organic polymers,[17] and we argued it might be equally effective in protecting the crystals from chemical degradation and structural collapse in water for a particularly delicate MOF. After incubation for 24 h, the PXRD of the crystals shows a clear influence on the concentration of CNTs over the structural stability of the framework when immersed in liquid water as a result of the formation of a denser shell (Figure 4d). Only TZDC-CNT-2 maintains its structural integrity compared to the collapse suffered by TZDC-CTN-1 and the pristine material This enhanced hydrolytic stability is also translated to the porosity of the crystals after the test (Figure 4e). Compared to CTN-2 which displays a SA of 4000 $m^2\ g^{-1}$, TZDC-CNT-1 and UiO-68-TZDC suffer from a reduction of ≈50 and ≈100% of the original value. To investigate the electrical conductivity of the composites, we contacted single crystals to a chip by using Pt wires and silver painting with futile results due to their small size (Section S5.3, Supporting Information). Instead, two-contact probe measurements of polycrystalline pellets revealed a bulk conductivity value of 4×10^{-2} S cm^{-1} for TZDC-CNT-2, compared to the insulating character of both CNT-1and the pristine MOF (Figure 4f). The poor homogeneity and conductivity displayed by a pellet prepared from a physical mixture of both components (2.3 wt.%) suggest the crucial role of covalent conjugation for their effective hybridization into a single crystal. Also, the steady-state emission spectrum of TZDC-CNT-2 after UV excitation (λ = 312 nm) shows a better-defined, more intense emission at 375 and 405 nm (Figure S28, Supporting Information), which suggests the creation of an interfacial Schottky barrier and results in higher quantum yields from

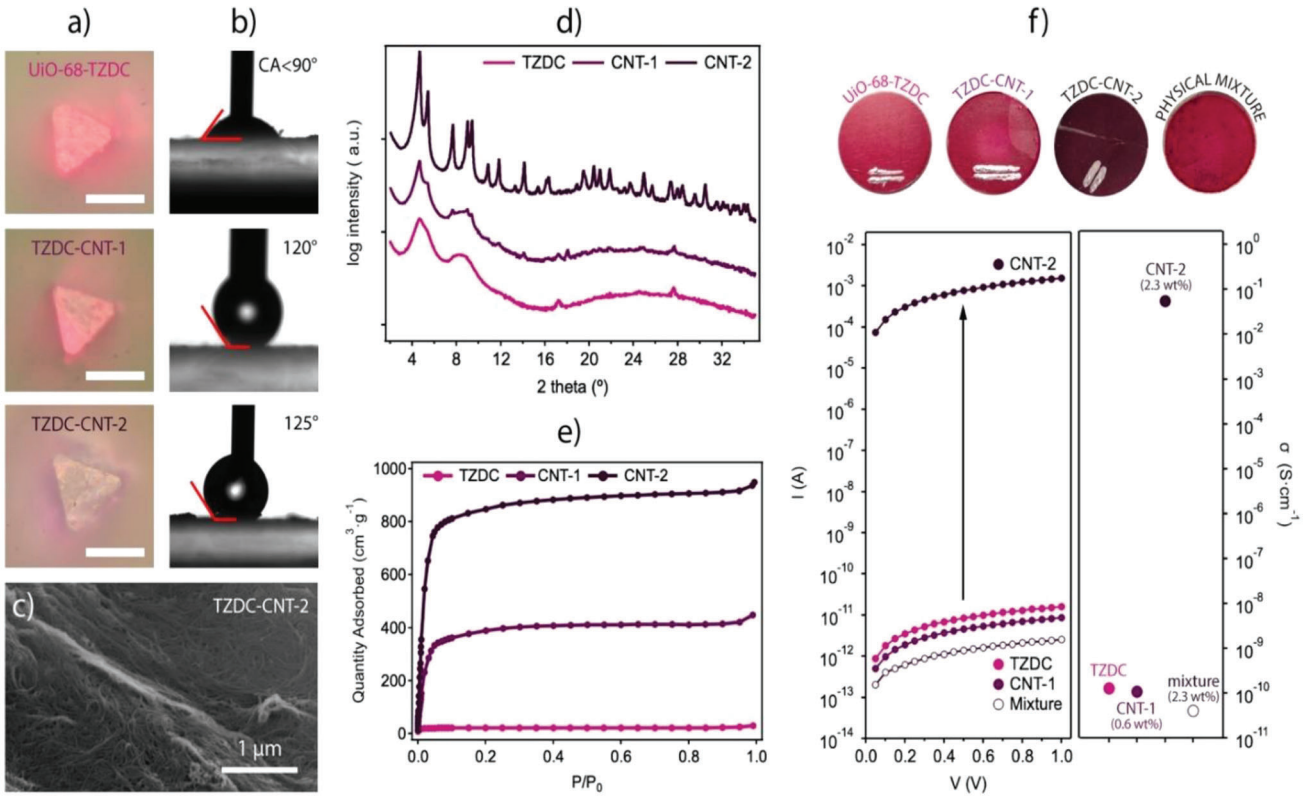

Figure 4. a) Crystals of UiO-68-TZDC, TZDC-CNT-1, and TZDC-CNT-2. Scale bars correspond to 15 µm. b) Contact angle measurements confirming their hydrophobicity after CNT linkage. c) SEM image of the crystal surface of CNT-2. d) PXRD and e) N_2 isotherms after incubation in water for 24 h showing the effect of the nanotube layer in protecting the crystals from chemical degradation and structural collapse. f) Pellets used for the transport measurements (top). *I–V* plots (left) and conductivity values (right) at room temperature.

decreasing recombination rates of photogenerated electron-hole pairs.[18]

3. Conclusion

Compared to other MOF/CNT composites,[10] TZDC-CNT-2 displays an optimal compromise between porosity, conductivity, and stability at very low carbon weight contents, thus offering an alternative for the design of MOF hybrid composites not reliant on their growth but adapted to controlled modification of the surface of preformed crystals. Following with our previous work in which electron-rich molecular dienophiles were used to functionalize post-synthetically the framework connectors for tailorable pore chemistry,[12] here we show how tetrazine chemistry can be extended from fullerene to other carbon nanoforms for similar click reactivity in mild conditions. For CNTs, diffusion inside the empty framework is limited by the size of the dienophile that imposes imposing surface functionalization. Based on the huge amount of work developed for over 15 years on the liquid-phase exfoliation[19] and functionalization of graphene[20] and inorganic graphenoids,[21] there is a huge pool of 2D nanosheets now available that, provided incorporation of electron-rich dienophiles to their surface, could be compatibilized with this same methodology. This would help build a chemical bridge between the realms of molecular frameworks and 2D materials for the design of multiple crystal composites.[22] We are confident this might offer unprecedented opportunities for exploiting the potential of reticular chemistry in applications as photovoltaics, sensing, electrocatalysis, thermoelectrics, or energy storage.

Supporting Information

Supporting Information is available from the Wiley Online Library or from the author.

Acknowledgements

B.L.-B. and N.M.P. contributed equally to the work. This work was supported by the EU H2020 program (ERC-2021-COG-101043428 & ERC-2016-STG-714122), the Generalitat Valenciana (PROMETEU/2021/054 and SEJIGENT/2021/059) and the Spanish government (CEX2019-000919-M, PID2020-118117RB-I00 & EUR2021-121999). B.L.-B. thanks the Spanish government for an FPU (FPU16/04162). N.M.P. and M.G. thanks La Caixa Foundation for a Postdoctoral Junior Leader–Retaining Fellowship (ID 100010434 & ID 100010434 and fellowship code LCF/BQ/PR20/11770014 & LCF/BQ/PR21/11840011). The authors also thank the University of Valencia for its research facilities (NANBIOSIS). J.A. and H. G. are grateful to the Spanish Ministry of Science and Innovation (RTI2018-98237-CO2-1) and Generalitat Valenciana (Prometeo 2021–038) for the financial support.

Conflict of Interest

The authors declare no conflict of interest.

Data Availability Statement

The data that support the findings of this study are available from the corresponding author upon reasonable request.

Keywords

carbon nanotubes, click chemistry, crystal hybrids, metal–organic frameworks, tetrazine tags

Received: February 26, 2023
Revised: May 23, 2023
Published online: June 19, 2023

[1] R. Freund, S. Canossa, S. M. Cohen, W. Yan, H. Deng, V. Guillerm, M. Eddaoudi, D. G. Madden, D. Fairen-Jimenez, H. Lyu, L. K. Macreadie, Z. Ji, Y. Zhang, B. Wang, F. Haase, C. Wöll, O. Zaremba, J. Andreo, S. Wuttke, C. S. Diercks, *Angew. Chem. Int. Ed* **2021**, *60*, 23946.
[2] H. Furukawa, K. E. Cordova, M. O'Keeffe, O. M. Yaghi, *Science* **2013**, *341*, 1230444.
[3] A. J. Howarth, Y. Liu, P. Li, Z. Li, T. C. Wang, J. T. Hupp, O. K. C. Farha, *Nat. Rev. Mater.* **2016**, *1*, 15018.
[4] O. Shekhah, J. Liu, R. A. Fischer, C. Wöll, *Chem. Soc. Rev.* **2011**, *40*, 1081.
[5] L. S. Xie, G. Skorupskii, M. Dincă, *Chem. Rev.* **2020**, *120*, 8536.
[6] V. Rubio-Giménez, S. Tatay, C. Martí-Gastaldo, *Chem. Soc. Rev.* **2020**, *49*, 5601.
[7] P. Ramaswamy, N. E. Wong, G. K. H. Shimizu, *Chem. Soc. Rev.* **2014**, *43*, 5913.
[8] T. Zhang, W. Lin, *Chem. Soc. Rev.* **2014**, *43*, 5982.
[9] Q.-L. Zhu, Q. Xu, *Chem* **2016**, *1*, 220.
[10] a) D. D. Chronopoulos, H. Saini, I. Tantis, R. Zbořil, K. Jayaramulu, M. Otyepka, *Small* **2022**, *18*, 2104628; b) J. E. Ellis, Z. Zeng, S. I. Hwang, S. Li, T.-Y. Luo, S. C. Burkert, D. L. White, N. L. Rosi, J. J. Gassensmith, A. Star, *Chem Sci* **2019**, *55*, 3566; c) S. J. Yang, J. Y. Choi, H. K. Chae, J. H. Cho, K. S. Nahm, C. R. Park, *Chem. Mater.* **2009**, *21*, 1893.
[11] M. Kalaj, K. C. Bentz, S. Ayala, J. M. Palomba, K. S. Barcus, Y. Katayama, S. M. Cohen, *Chem. Rev.* **2020**, *120*, 8267.
[12] B. Lerma-Berlanga, C. R. Ganivet, N. Almora-Barrios, R. Vismara, J. A. R. Navarro, S., M. Tatay, N. Padial, C. Martí-Gastaldo, *Angew. Chem., Int. Ed.* **2022**, *61*, 202208139.
[13] B. Lerma-Berlanga, C. R. Ganivet, N. Almora-Barrios, S. Tatay, Y. Peng, J. Albero, O. Fabelo, J. González-Platas, H., M. García, N. Padial, C. Martí-Gastaldo, *J. Am. Chem. Soc.* **2021**, *143*, 1798.
[14] F. I. Pambudi, *Crystal Growth of Metal–Organic Frameworks Investigated by Atomic Force Microscopy*, Ph.D. Thesis, University of Manchester, **2019**.
[15] J. L. Delgado, P. de Cruz, F. Langa, A. Urbina, J. Casado, J. T. L. Navarrete, *Chem. Commun.* **2004**, 1734.
[16] R. Graupner, *J. Raman Spectrosc.* **2007**, *38*, 673.
[17] K. Jayaramulu, F. Geyer, A. Schneemann, Š. Kment, M. Otyepka, R. Zboril, D. Vollmer, R. A. Fischer, *Adv. Mater.* **2019**, *31*, 1900820.
[18] K. Woan, G. Pyrgiotakis, W. Sigmund, *Adv. Mater.* **2009**, *21*, 2233.
[19] V. Nicolosi, M. Chhowalla, M. G. Kanatzidis, M. S. Strano, J. N. Coleman, *Science* **2013**, *340*, 1226419.
[20] C. Wetzl, A. Silvestri, M. Garrido, H. Hou, A. Criado, M. Prato, *Angew. Chem., Int. Ed.* **2023**, *62*, 202212857.
[21] G. Bottari, M. Á. Herranz, L. Wibmer, M. Volland, L. Rodríguez-Pérez, D. M. Guldi, A. Hirsch, N. Martín, F. D'Souza, T. Torres, *Chem. Soc. Rev.* **2017**, *46*, 4464.
[22] E. Pomerantseva, F. Bonaccorso, X. Feng, Y. Cui, Y. E. S. Gogotsi, *Science* **2019**, *366*, 6468.